

A NUMERICAL MODEL OF HERCULES A BY MAGNETIC TOWER: JET/LOBE TRANSITION, WIGGLING, AND THE MAGNETIC FIELD DISTRIBUTION

MASANORI NAKAMURA¹, IAN L. TREGILLIS², HUI LI¹, AND SHENGTAI LI³

Draft Version Jun. 17, 2008: Accepted for Publication in ApJ

ABSTRACT

We apply magnetohydrodynamic (MHD) modeling to the radio galaxy Hercules A for investigating the jet-driven shock, jet/lobe transition, wiggling, and magnetic field distribution associated with this source. The model consists of magnetic tower jets in a galaxy cluster environment, which has been discussed in a series of our papers. The profile of underlying ambient gas plays an important role in jet-lobe morphology. The balance between the magnetic pressure generated by axial current and the ambient gas pressure can determine the lobe radius. The jet body is confined jointly by the external pressure and gravity inside the cluster core radius R_c , while outside R_c it expands radially to form fat lobes in a steeply decreasing ambient thermal pressure gradient. The current-carrying jets are responsible for generating a strong, tightly wound helical magnetic field. This magnetic configuration will be unstable against the current-driven kink mode and it visibly grows beyond R_c where a separation between the jet forward and return currents occurs. The reversed pinch profile of global magnetic field associated with the jet and lobes produces projected \mathbf{B} -vector distributions aligned with the jet flow and the lobe edge. AGN-driven shock powered by the expanding magnetic tower jet surrounds the jet/lobe structure and heats the ambient ICM. The lobes expand subsonically; no obvious hot spots are produced at the heads of lobes. Several key features in our MHD modeling may be qualitatively supported by the observations of Hercules A.

Subject headings: galaxies:individual: Hercules A — galaxies: active — galaxies: jets — methods: numerical — MHD

1. INTRODUCTION

In the present paper, we continue our discussion of the dynamics of extragalactic jets in cluster environments within the framework of the “magnetic tower” model (Lynden-Bell & Boily 1994; Lynden-Bell 1996), which we have analyzed in a series of papers. Magnetohydrodynamic (MHD) mechanisms are frequently invoked to model the launching, acceleration and collimation of astrophysical jets (see, *e.g.*, Ferrari 1998; Meier et al. 2001, and references therein). An underlying large-scale (coronal) poloidal field for producing the magnetically driven jets is almost universally assumed in many theoretical/numerical models. However, the origin and existence of such a galactic magnetic field are still poorly understood.

In contrast with the large-scale field models, Lynden-Bell (Lynden-Bell & Boily 1994; Lynden-Bell 1996) examined the expansion of the local force-free magnetic loops anchored to the star and the accretion disk by using the semi-analytic approach. Twisted magnetic fluxes due to the disk rotation make the magnetic loops unstable and splay out at a semi-angle 60° from the rotational axis of the disk. Global magnetostatic solutions of magnetic towers with external thermal pressure were also computed by Li et al. (2001) using the Grad-Shafranov equation in axisymmetry (see also, Lovelace et al. 2002; Lovelace & Romanova 2003; Uzdensky & MacFadyen 2006). Full MHD numerical simulations of magnetic towers have been performed in two-dimension (axisymmetric) (Romanova et al. 1998; Turner et al. 1999; Ustyugova et al. 2000; Kudoh et al.

2002; Kato et al. 2004) and three-dimension (Kato et al. 2004). Magnetic towers are also observed in laboratory experiments (Hsu & Bellan 2002; Lebedev et al. 2005).

The first in our series, Li et al. (2006, hereafter Paper I), described the basic assumptions and approaches in the numerical modeling of magnetic tower jets. The evolution of the tower jets in a constant density/pressure background was examined there. The second in our series, Nakamura et al. (2006, hereafter Paper II) investigated the global structure of magnetic tower jets in a gravitationally-stratified atmosphere, in terms of the MHD wave structure, radial force equilibrium, and collimation. A large current flowing parallel to the jet bulk flow plays an essential role in the determining the lobe radius, as does the background pressure profile. The third in our series, Nakamura et al. (2007, hereafter Paper III) investigated the stability properties of magnetic tower jets on cluster scales. Current-driven instabilities are responsible for the non-axisymmetric structures; the external “kink” ($m = 1$) mode grows outside R_c , while the internal “double helix” ($m = 2$) mode grows predominantly inside R_c . This is the forth in our series of papers to examine the nonlinear magnetic tower jets. Here we examine our model’s applicability to an individual source, Hercules (Herc) A (3C 348), by performing three-dimensional MHD simulations.

Herc A is one of the most powerful double-lobed radio sources in the sky. Its total energy content is approximately 3×10^{60} erg and it is identified with the central compact diffuse (cD) galaxy of a cluster (Sadun & Hayes 1993) at a low redshift of $z = 0.154$ (Siebert et al. 1999). The X-ray luminosity of 4.8×10^{44} erg s^{-1} (Gizani & Leahy 2004) is thought to be due to bremsstrahlung of the very high temperature intracluster medium (ICM). Herc A has a peculiar radio structure; the morphology looks like a classical double-lobed Fanaroff-Riley type II (FR II) radio source (Fanaroff & Riley 1974), but it has no compact hotspots, in-

¹ Theoretical Astrophysics, MS B227, Los Alamos National Laboratory, NM 87545; nakamura@lanl.gov

² Applied Physics, MS F699, Los Alamos National Laboratory, NM 87545

³ Mathematical Modeling and Analysis, MS B284, Los Alamos National Laboratory, NM 87545

stead showing an unusual jet-dominated morphology as in an Fanaroff-Riley type I (FR I) radio source, which was first revealed by Dreher & Feigelson (1984). Furthermore, the two jets in Herc A are quite different in appearance. The eastern jet appears to have continuous twisting flows, while the western jet leads to a unique sequence of “rings”. The jets in Herc A are well-collimated initially but they flare suddenly at a certain distance from the nucleus. An explanation for the presence of such different structures in the same source is still unresolved in the literature. Herc A is not a typical FR I source, either; its jets are well-collimated and has knot components. Therefore, Herc A might be classified an intermediate case: FR I/II.

Various models have been proposed for explaining the formation of the jets and rings in Herc A, including both kinematic (Mason et al. 1988; Morrison & Sadun 1996; Sadun & Morrison 2002) and dynamic (Meier et al. 1991; Saxton et al. 2002) points of view. By performing axisymmetric, two-dimensional hydrodynamic simulations, Meier et al. (1991) proposed a model in which an *over*-dense and *over*-pressured jet undergoes a sudden expansion when it becomes highly over-pressured compared to the background gas at a certain distance from the core. This causes a subsequent conical expansion, giving rise to the “ice cream cone” shape of the lobe. However, at present, there is nothing in the X-ray observations to suggest that the jet becomes thermally over-pressured as required in this model. In Saxton et al. (2002), the formation of ring structure in the western jet is interpreted as the result of ribbon-like, annular shocks propagating through the jet cocoon. Also, these authors conclude that the absence of hot spots in Herc A results from the dynamics of turbulent and entraining backflows in the radio lobe.

Recently, Gizani & Leahy (2003) have revealed detailed structures of total intensity, spectral index, polarization, and projected magnetic field in Herc A by using multifrequency VLA imaging. The jet disruption in the eastern lobe is clearly visible, implying flow instabilities. The projected magnetic field, after correcting for Faraday rotation, closely follows the edges of the lobes, the jets, and the rings; the two lobes have generally similar field patterns. This observational picture may disagree with the turbulent structure inside the lobes suggested by Saxton et al. (2002).

Magnetic field distributions associated with the extragalactic jets and their comparisons with the observations have been examined by using Stokes parameters, Faraday rotation measure (RM), and the projected magnetic field (\mathbf{B} -vector) (e.g., Laing 1981; Clarke et al. 1989, 1992; Hardee & Rosen 1999, 2002; Laing et al. 2006). In general, helical magnetic fields produce asymmetric transverse brightness and polarization profiles; they are symmetrical only if the field is purely toroidal or the jet is at 90° to the line of sight (Laing 1981). Laing et al. (2006) conclude that, to the first approximation, the field configuration in FR I jet over 10 kpc scales is a mixture of toroidal and longitudinal components.

Gizani & Leahy (2004)’s *ROSAT* X-ray observations of the intracluster gas in the Herc A cluster have revealed extended X-ray emission coming from a compact source at the center of cluster, out to a radius of 2.2 Mpc. The azimuthally-averaged X-ray surface brightness profile is well fitted by a modified King (β) model (King 1972; Cavaliere & Fusco-Femiano 1976), with core radius $R_c = 121 \pm 10$ kpc and $\beta = 0.74 \pm 0.03$. Their X-ray analysis supports the conclusion that the inner jets are confined thermally by the cluster core gas: thermal pressure in the cluster core is almost 10 times

larger than the equipartition pressure in the eastern jet with the standard assumptions (including no protons). The radio lobes are largely positioned *beyond* the X-ray core radius, allowing for projection, so they are expanding essentially into a power-law atmosphere with density falling as $R^{-3\beta} \sim R^{-2.22}$, quite close to the R^2 profile needed to give the lobes a self-similar structure (Falle 1991).

These observational evidence motivate us to apply our dynamical magnetic tower jet model to Herc A. To our knowledge, no MHD model has been applied to Herc A before though there are several hydrodynamic models as we have already referred. Radio observations suggest that the magnetic fields need to be taken into account to discuss about jet/lobe dynamics in Herc A. We believe that a key clue to understanding the transition between the jet and the lobe may be whether or not the inner jets become over-pressured during their propagation in the X-ray thermal cluster gas. However, the jet internal pressure may be magnetically, rather than thermally, dominated. This is in contrast to previous models (Meier et al. 1991). Of particular interest here are the jet/lobe transition, wiggling, and the magnetic field distribution associated with the eastern jet of Herc A, which are not yet fully discussed among the past hydrodynamic models of Herc A. We do not discuss the formation of rings in the western jet in this paper.

This paper is organized as follows. In §2, we outline our numerical methods. In §3, we describe our numerical results. Discussions and conclusions are given in §4 and §5.

2. NUMERICAL METHODS AND MODEL ASSUMPTIONS

We solve the nonlinear system of time-dependent ideal MHD equations numerically in a 3-D Cartesian coordinate system (x, y, z) . The basic numerical treatments (including the MHD numerical scheme) is essentially the same as that in Papers I - III. We assume an initial hydrostatic equilibrium in the gravitationally stratified medium, adopting an isothermal King model. The magnetic flux and the mass are steadily injected in a central small volume during a certain time period. Since the injected magnetic fields are not force-free, they will evolve as a “magnetic tower” and interact with the ambient medium. The dimensionless system of MHD equations is integrated in time by using the TVD upwind scheme (Li & Li 2003). Computations were performed on the parallel Linux clusters at the Los Alamos National Laboratory.

2.1. Numerical Set Up

We normalize physical quantities with the unit length scale R_0 , the unit density ρ_0 , and the sound speed C_{s0} as the typical speed in the system. Other quantities are derived from their combinations, e.g., the typical time t_0 is R_0/C_{s0} , etc. In this paper, we use some observed quantities associated with the source Herc A (Gizani & Leahy 2004, hereafter GL04) in order to determine our normalization units. A central electron density $n_e = 1.0 \times 10^{-2} \text{ cm}^{-3}$ is adopted in GL04, suggesting quite a dense cluster, as such densities in clusters are typically of order 10^{-3} cm^{-3} (Jones & Forman 1984). This provides a unit density $\rho_0 = 1.7 \times 10^{-26} \text{ g cm}^{-3}$. A single-temperature fit with $kT = 4.25 \text{ keV}$ is assumed for the β -model cluster, giving a unit temperature $T_0 = 4.9 \times 10^7 \text{ K}$, a unit pressure $p_0 = 2.3 \times 10^{-10} \text{ dyn cm}^{-2}$, and a unit velocity (sound speed) $C_{s0} (\equiv \gamma p_0 / \rho_0) = 1.2 \times 10^8 \text{ cm s}^{-1}$. Here, we choose a unit length $R_0 = 30 \text{ kpc}$, and therefore, a unit time $t_0 = 2.4 \times 10^7 \text{ yr}$. The unit magnetic field B_0 is $(4\pi\rho_0 C_{s0}^2)^{1/2} = 53.4 \mu\text{G}$.

In the King model we use here, we take the cluster core radius R_c to be 120 kpc, corresponding to the normalized core radius 4.0, and take the exponential slope κ to be 1.1 ($3\beta/2$ with $\beta = 0.74$) by adopting the observations in GL04.

We use ρ_0 and p_0 as the initial quantities at the origin $(x, y, z) = (0, 0, 0)$ and thus, the normalized ρ and p are set to unity at the origin in these simulations. The total computational domain is taken to be $|x|, |y|, |z| \leq 15$. The number of grid points in the simulations reported here is 360^3 , where the grid points are assigned uniformly in the x, y , and z directions. The simulation domain is from -450 to 450 kpc, with $\Delta x = \Delta y = \Delta z \sim 0.083$, which correspond to ~ 2.5 kpc.

The injections of magnetic flux, mass, and the associated energies are the same as those described in Paper I. The ratio between the toroidal to poloidal fluxes of the injected fields is characterized by a parameter $\alpha = 25$. The magnetic field injection rate is described by γ_b and is set to be $\gamma_b = 1$. The mass is injected at a rate of $\gamma_\rho = 0.1$ over a central volume with a characteristic radius $r_\rho = 0.5$. Magnetic fluxes and mass are continuously injected for $t_{\text{inj}} = 3.0$, after which the injection is turned off. These parameters correspond to a magnetic energy injection rate of $\sim 2.7 \times 10^{46}$ ergs s^{-1} and an injection time ~ 72 Myrs. The energy injection rate used here is a similar range to that of other hydrodynamic simulations with the jet power $2 \times 10^{45-46}$ ergs s^{-1} (Saxton et al. 2002). We use the outflow boundary conditions at all outer boundaries. Note that for most of the simulation duration, the waves and magnetic fields stay within the simulation box, and all magnetic fields are self-sustained by their internal currents.

2.2. Formulation of Synthetic Observation Images

Based on our simulations, we make synthetic observation images to compare with the real observations of Herc A (Gizani & Leahy 2003, hereafter GL03). The synthetic radio telescope observations presented here were produced using a modified form of the synthetic observation technique first described in Tregillis et al. (2001). Here we provide an overview of the key points relevant to the present investigation; a complete description of the technique is provided in Tregillis (2002).

Our method utilizes the vector magnetic field structures evolved self-consistently within these MHD calculations and a relativistic-electron momentum distribution, $f(p)$, chosen by fiat during postprocessing. The function $f(p)$ is defined over eight logarithmically-spaced momentum bins. Each bin has an associated slope value, q , and within each bin the distribution is a power law ($f \sim p^{-q}$). Slope values may vary between bins, however, making it possible to specify non-power law distributions, such as would be appropriate for cases where radiative aging is significant. The specified distribution functions are free to vary from location to location within the simulated flows, as is expected to be the case in real radio galaxies. We note that although these distributions are not derived self-consistently within the computed flows, as has been done in previous works (Tregillis et al. 2001, 2004), imposing it as a postprocessing step does provide a measure of flexibility in our investigations.

In this paper we choose the sign convention such that $\alpha > 0$, and the flux density $S_\nu \propto \nu^{-\alpha}$. For the present investigations, which do not incorporate the effects of radiative aging and reacceleration, we applied a spatially-uniform momentum slope value $q = 4.5$ throughout the simulated source. This corresponds to a synchrotron spectral index $\alpha = 0.75$, which is consistent with the observed range of spectral indices within

individual radio galaxies. For example, Gizani & Leahy (2003) mapped the spectral index distribution in Herc A between 1.3 and 4.8 GHz, finding $0.6 \lesssim \alpha_{1.3}^{4.8} \lesssim 2.0$, with the flattest values within the western jet and the steepest values along the lobe edges. They also found $\alpha_{1.3}^{4.8} \approx 0.75$ in portions of the eastern jet. Our choice, $\alpha = 0.75$, is also consistent with typical hotspot spectral index values $\alpha_{1.4}^{5.0}$ in the sample of 3CR sources studied by Alexander & Leahy (1987).

The local number density of energetic electrons varied with the local magnetic energy density (i.e., $n_e \propto B^2$). This approach represents a partitioning relationship between the field and particle energies, such as is posited by minimum-energy arguments (Miley 1980). However, the overall scaling was chosen such that the energy density of relativistic electrons was far less than the magnetic energy density (i.e., we assume our simulated object is out of equipartition, which is consistent with the lack of dynamical feedback from the electrons in these calculations).

Given information about the local magnetic field and the local distribution of energetic electrons, we compute a synchrotron emissivity j_ν in every zone of the computational grid. As given by Jones et al. (1974), the emissivity is

$$j_s(\nu) = j_{\alpha 0} \frac{4\pi e^2}{c} f(p_s) p_s^q \left(\frac{\nu_{B_\perp}}{\nu} \right)^\alpha \nu_{B_\perp}. \quad (1)$$

The spectral index α is related to the local electron momentum index q via $\alpha = (q-3)/2$, $\nu_{B_\perp} = eB \sin \Omega / (2\pi m_e c)$, where Ω projects the local field onto the sky, and $j_{\alpha 0}$ is an order-unity dimensionless constant, defined in Jones et al. (1974). For a selected observing frequency, ν , the distribution, $f(p_s)$, and the index, q , are determined for each point on the numerical grid by establishing the relevant electron momentum from the relation $p_s = [2\nu / (3\nu_{B_\perp})]^{(1/2)}$, with p_s in units $m_e c$.

Once the synchrotron emissivity is known for every numerical zone, we compute surface brightness maps for optically-thin emission via line-of-sight integrations. Similarly, we can obtain the Stokes Q and U parameters for the synchrotron emission, as well as the correction for Faraday rotation through the source, making detailed polarimetric studies possible. We write the resultant data in FITS format, and analyze it using conventional observational packages (MIRIAD and KARMA (Gooch 1995)).

3. RESULTS

Our magnetic tower model has been applied to the Herc A. In particular, our goal is to reproduce large scale structures in the jets: the jet/lobe transition, the non-axisymmetric deformation, and the projected magnetic field distribution associated with the jets and lobes, as observed in GL03.

Figure 1 shows a snapshot of the gas pressure p in the $(x-z)$ cross section at $t = 8.0$ (192 Myr). As we have examined in papers II and III, the global structure of the magnetic tower consists of a well-collimated ‘‘body’’ and radially extended ‘‘lobes’’ in the gravitationally stratified atmosphere. A transition from the narrow jet to the fat lobe can occur at the cluster core radius. This interesting property can be confirmed in recent observations (GL03, GL04). Several key features in these magnetic tower jets (the MHD wave structures, the heating process at the tower front, the cylindrical radial force equilibrium at the tower edge, and the dynamic collimation process) are similar to the results of paper II (see also Fig. 1 of paper II for details of time evolution). The helically-twisted magnetic tower has a closed current system that includes a pair of current circuits. Each circuit contains a forward electric current path (the jet flow itself, with its toroidal magnetic field,

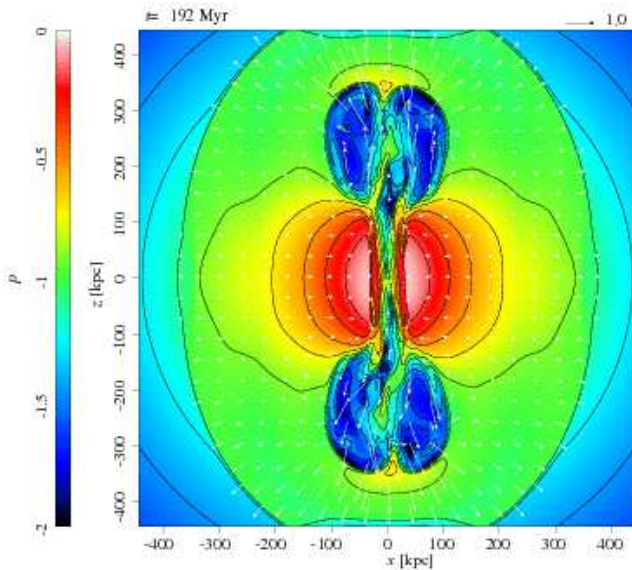


FIG. 1.— Distribution of the gas pressure p (logarithmic scale) with the velocity field (V_x , V_z) (arrows) in the $x-z$ plane at 192 Myr. The length and time scales are converted into the corresponding dimensional values. The cavities (low density and gas pressure) are formed due to the magnetic tower expansion as corresponding lobes. The jets are deformed into the wiggled structures inside the lobes.

toward the lobe) and a return current (along some path back to the AGN core). The global picture of a current-carrying jet with a closed current system linking the magnetosphere of the central engine and the hot spots was introduced by Benford (1978, 2006) and applied to AGN double radio sources. As seen in Fig. 1, the high-pressure material of the ambient gas seems to follow the edge of the jet near the bottom of each lobe. However, this is not the case, but the local pressure enhancement occurs inside the lobes. In the jet and lobe system, the axial currents drive the current-driven instabilities; it eventually produces magnetic reconnection process even in our ideal MHD assumption (the magnetic field will dissipate numerically). As a result, some local heating may occur, but it never affects the dynamics of jet propagation dramatically.

For a full 3-D visualization of the magnetic lines of force, the reader is referred to paper III. The basic behavior of the helically-twisted magnetic field in the present paper appears similar to that in paper III. The magnetic tower jet has a well-ordered helical field configuration, with a tightly-wound central helix going up along the central axis and a loosely-wound helix coming back at the outer edge of the magnetic tower. The outer edge of the magnetic tower may be identified as a tangential discontinuity without the normal field component. The interior of tower (lobe) is separated from the non-magnetized external gas via this discontinuity. At the tower edge, the outward-directed magnetic pressure gradient force is roughly balanced with the inwardly-directed thermal pressure gradient force. On the other hand, at the core part of jet body, a quasi-force free equilibrium is achieved. In the context of magnetically-controlled fusion systems, the helical field in the magnetic tower can be regarded as the reversed field pinch (RFP) profile.

The jet axial current and the ambient gas pressure can together determine the radius of the magnetically-dominated lobes (paper II). That is, the internal gas pressure plays a mi-

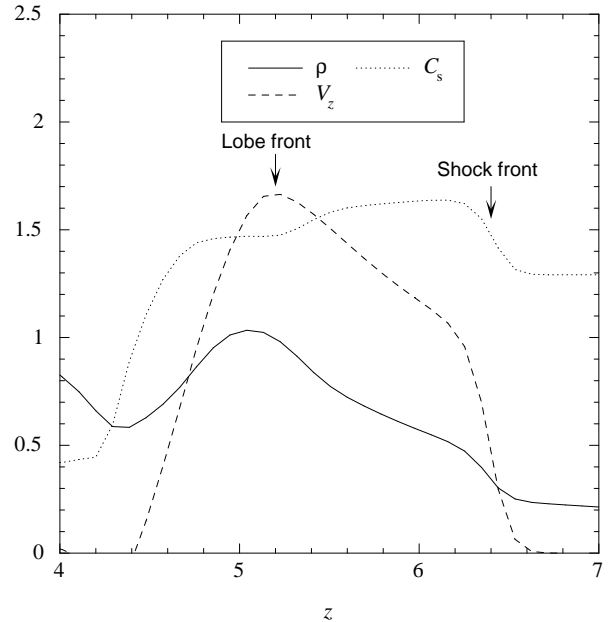


FIG. 2.— Axial profiles of physical quantities along the z -axis at $t = 3.0$ ($t = 72$ Myrs). Density ρ , sound speed C_s , and the axial velocity component V_z . The positions of the expanding shock and lobe fronts are shown.

nor role in the lobes (even if the thermal pressure is greater than the non-thermal pressure (Morganti et al. 1988) as is typically seen in FR I radio galaxies (Croston et al. 2003). The Alfvén speed becomes large (about three times the local sound speed), while the plasma β ($\equiv 2p/B^2$) becomes small ($\beta \lesssim 0.1$) inside the density cavities due to the expansion of magnetic fluxes. As we have already discussed in paper II, it is remarkably noted that the expanding tower launches a preceding hydrodynamic shock in the ICM, which may be associated with AGN-driven shocks seen in recent X-ray observations (Forman et al. 2005; Nulsen et al. 2005; Fabian et al. 2006).

Figure 2 exhibits physical quantities along the z -axis at $t = 3.0$ ($t = 72$ Myrs). The magnetic tower-driven hydrodynamic shock front can be seen around $z \sim 6.4$ in the profiles of ρ , C_s , and V_z . The sound speed jumps by 27% [the temperature $T \propto C_s^2$ increases by 61%] in the post-shocked region due to the shock compression. The magnetic tower front, which is identified as the lobe front, is located at $z \sim 5.2$. There is another MHD wave front at $z \sim 4.5$ where an increase in C_s (density/pressure also) is accompanied by an increase in magnetic pressure (not shown in Fig. 2), indicating the reverse MHD slow mode. In later time, this can steepen into a MHD slow shock that cause a compression (heating) at the head of magnetic tower as seen in Fig. 1 (see also Fig. 2 and §3.1 of paper II for details).

Figure 3 displays the positions of the shock and lobe fronts as a function of time along the z -axis (propagating towards the positive direction). The shock front has a constant propagation speed $V_{SH} \sim 2.1$ (2.52×10^8 cm s $^{-1}$) that implies a Mach number ~ 1.63 . On the other hand, the magnetically-dominated lobe front expands subsonically. This lobe front also has a quasi-constant propagation speed $V_{LB} \sim 1.5$ (1.8×10^8 cm s $^{-1}$) that implies a Mach number ~ 0.91 (C_s increases up to ~ 1.64 in shocked ICM; see also Fig. 2).

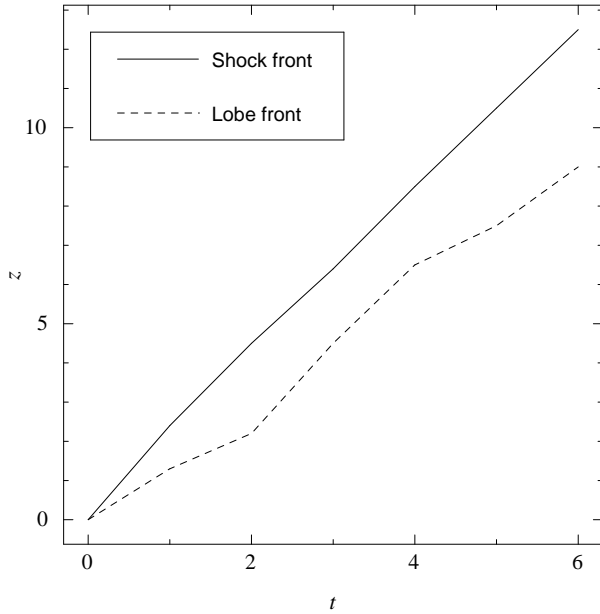


FIG. 3.— The temporal evolution of the shock and lobe front positions along the z -axis. During the time evolution, both fronts propagate with almost constant speeds. The shock front expands supersonically with Mach number ~ 1.63 (relative to the unshocked ICM), while the lobe front proceeds subsonically with Mach number ~ 0.9 (relative to the shocked ICM cocoon).

The current-carrying magnetic tower jet, which possesses a highly-wound helical field, is subject to the current-driven instability (CDI). Although the destabilization criteria will be modified by the ambient gas and the RFP configuration of the tower, we find that the propagating magnetic tower jets can develop the non-axisymmetric CDI modes. As seen in Fig. 4, both the internal elliptical ($m = 2$) mode like the “double helix” and the external kink ($m = 1$) mode grow to produce the wiggles at different locations (see also paper III for details). We see no disruption owing to shear-driven, Kelvin-Helmholtz modes and/or the pressure-driven interchange modes.

Figure 5 shows the synthetic radio synchrotron intensity at 5 GHz, along with the polarization magnetic field vectors. The wiggled structures can be observed in both the jet and lobe. Also, filamentary structures appear beyond R_c . The projected magnetic field is aligned with the jet and along the lobe edge. The magnetic tower model produces polarization features that are qualitatively consistent with those seen in the Herc A observations of GL03. Furthermore, our dynamical solution of magnetic tower’s evolution may give a self-consistent explanation to a feasible magnetic configuration discussed in non-dynamical models having “spine” ($B_\phi > B_z$ inside the lobe) – “Sheath” ($B_z > B_\phi$) structure in FR I jet over 10 kpc scale as discussed in Laing (1981); Laing et al. (2006).

The image contrast in our synthetic synchrotron surface-brightness map is approximately 2000:1 between the brightest pixels (beams) near the central core and the faintest regions inside the lobes. Outside the small bright core region, the image contrast is roughly 200:1.

When the synthetic 5 GHz synchrotron map is scaled to an angular size comparable to that of Herc A, the brightest

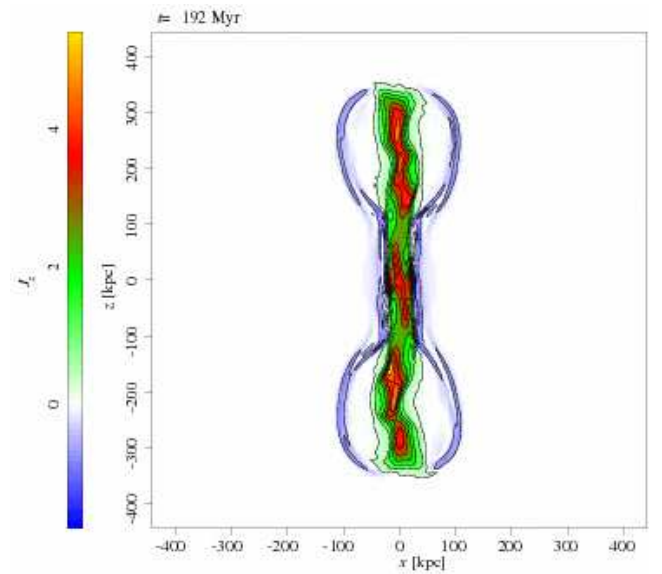


FIG. 4.— Distribution of the axial current density J_z in the $x-z$ plane at the same time as Fig. 1. Two types of growing current-driven (external/internal) modes are visible in the lobe and jet.

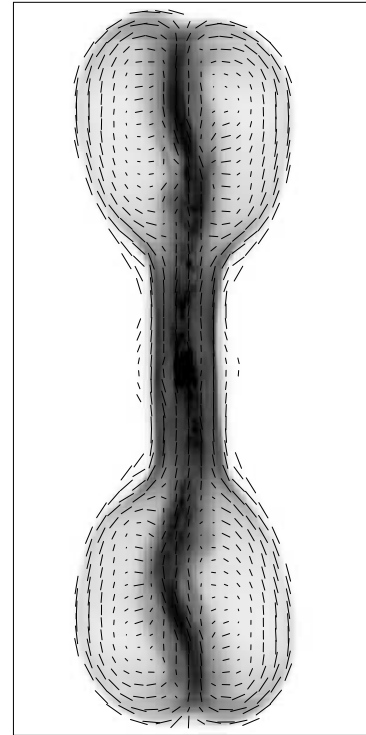


FIG. 5.— Synthetic synchrotron surface brightness computed at 5 GHz (greyscale), overlaid with polarization magnetic field vectors. The field vectors are corrected for Faraday rotation, and represent the field orientations at the source. The polarization field is nicely aligned with the jets and lobe edges.

pixel (beam) in the synthetic 5 GHz surface brightness map is 875 mJy/beam. However, away from the small, bright region near the core, the jets generally exhibit flux densities on the order of 30-70 mJy/beam, the central sheath exhibits flux densities in the range 20-30 mJy/beam, and the darkest parts

of the lobes exhibit $\lesssim 1.0$ mJy/beam.

Our simulated source exhibits a fractional linear polarization, m , at 5 GHz ranging from a few percent in the most magnetically tangled portions of the lobes to $m \approx 30 - 50\%$ on the lobe edges. These values are consistent with those typically observed in radio galaxies (Bridle & Perly 1984; Muxlow & Garrington 1991) as well as with the m values reported in GL03 for Herc A at 4848 MHz. Fractional polarization values exceed 60% (roughly twice that reported in GL03) in small, isolated pockets in the sheath around the central jet and near the central core, which may indicate insufficient computational resolution near the core for properly capturing cellular depolarization. In regions outside the magnetized lobes, where the ambient medium in our calculational domain has been mildly perturbed by expansion of the magnetic tower, the degree of polarization approaches 72%. This is the expected result for a region with a uniform magnetic field and a uniform power-law distribution of nonthermal electrons with $q = 4.5$ (Rybicki & Lightman 1979).

4. DISCUSSION

4.1. Shock and Lobe Expansions

Some features about the shock and lobe expansions in the simulation are discussed by comparing with observations. A *Chandra* X-ray image of the Herc A cluster shows that it has cavities and a shock front associated with the powerful radio lobes (Nulsen et al. 2005). Unusually, these cavities show no clear connection to the radio sources, while many cavities are associated with radio sources in other cluster cases (e.g., McNamara et al. 2000), indicating that they might be ghost cavities (e.g., McNamara et al. 2001).

Nulsen et al. (2005)'s observation reveals that a shock front surrounds the Herc A radio source. It is elongated in the direction of the radio lobes and appears to be a cocoon shock (Scheuer 1974). Their fitting of a simple hydrodynamic model to the surface brightness profile gives a Mach number for the shock front of ~ 1.65 and its total energy $\sim 3 \times 10^{61}$ ergs (its mean mechanical power $\sim 1.6 \times 10^{46}$ ergs s^{-1}) is estimated. As we examined in §3, the magnetic tower drives a hydrodynamics shock front in the ambient ICM. Derived Mach number $M \sim 1.63$ matches quite well to their observation and also our energy inputs are in qualitatively reasonable range.

As the radio lobes of Herc A lack anything resembling hotspots, it seems likely that they are expanding at around the sound speed, and so are confined by the thermal pressure of the ambient ICM, rather than by strong shocks (Gizani & Leahy 2004). To our knowledge, there may be no direct result revealing the lobe expansion speed of Herc A radio lobes, but we discuss general properties of expanding lobes in radio galaxy based on Kraft et al. (2006)'s argument. It is believed that the radio lobes are greatly overpressurized relative to the ambient medium, indicating that sharp X-ray surface brightness discontinuities or large jumps in gas temperature at the lobe edges. A high Mach number ($M \sim 8.5$) shock is detected around the SW radio lobe of Centaurus A (Kraft et al. 2003).

However, there is no evidence especially for FR I or low-power FR II radio galaxies, including Herc A (Gizani & Leahy 2004) and 3C 388 (Kraft et al. 2006). If thermal conduction in the ICM is efficient (an order of the Spitzer value), then shocks may be nearly isothermal and thus difficult to detect (Fabian et al. 2006). However, *Chandra* observations suggest that the thermal conduction (and viscos-

ity) of the ICM is orders of magnitude below the Spitzer value (e.g., Vikhlinin et al. 2001; Kraft et al. 2003). Thus, some lobes including Herc A may be inflating transonically and subsonically (i.e., $M \leq 1$). Based on hydrodynamic arguments of a buoyant bubble, $M \sim 0.6$ in M87 (Churazov et al. 2002) and $M \sim 0.5 - 0.9$ in 3C 388 (Kraft et al. 2006) are estimated. Our numerical result indicates that the magnetically-dominated lobe expands subsonically with $M \sim 0.91$, discussed in §3. This will also match the observationally preferable picture.

4.2. Lobe Size

We next discuss the radial size of the lobes r_{lobe} as based on our model (Nakamura et al. 2006). The poloidal magnetic fluxes and the poloidal current I_z in the lobes remain well collimated around the central axis even after the system has evolved fully. This implies that the toroidal magnetic fields in the lobe region are distributed roughly as

$$B_\phi \sim I_z/r. \quad (2)$$

When the lobe experiences sufficient expansion, we can expect $|B_z| \sim |B_\phi|$ at the outer edge of the RFP configuration (Freidberg 1982). The magnetic and background pressures tend to balance each other at the tower edge. Thus, we can expect that

$$\frac{B_\phi^2 + B_z^2}{2} \sim B_\phi^2 \sim p_e, \quad (3)$$

where p_e is the external gas pressure at the tower edge. By combining eqs. (2) and (3), we have

$$B_\phi^2 \sim \left(\frac{I_z}{r_{\text{lobe}}} \right)^2 \sim p_e, \quad (4)$$

which gives

$$r_{\text{lobe}} \sim I_z p_e^{-1/2}. \quad (5)$$

Figure 6 shows the distribution of p along a transverse line at $z = 8.5$ (255 kpc), when the lobe has a maximum radius (after 192 Myr, as in Figs. 1 and 4). We can see that the external gas pressure begins to decrease around $x \sim 5$ (150 kpc) toward the central (z) axis. The pressure cavity corresponds to the lobe of our magnetic tower. We can estimate the lobe radius r_{lobe} predicted by eq. (5) from physical quantities in simulation. From Fig. 2, we take $J_z \sim 3$ (4.5×10^{-24} A/cm $^{-2}$) within a radius $r \sim 0.75$ (22.5 kpc), which makes $I_z \sim 1.68$ (5×10^{17} A). As suggested by Fig. 4, we estimate $p_e \sim 0.11$ (2.5×10^{-11} dyn cm $^{-2}$) for the external gas pressure. We therefore obtain $r_{\text{lobe}} \sim 5.2$ or roughly 156 kpc. Thus, we find that the depression radius in Fig. 6 is qualitatively consistent with r_{lobe} and is comparable with the physical scale seen in radio observations (Gizani & Leahy 2003). Based on this numerical result, we estimate that one simulated lobe of Herc-A may contain a total energy $\sim 1.8 \times 10^{61}$ ergs, out of which $\sim 1.0 \times 10^{61}$ ergs are in magnetic energy, $\sim 1.4 \times 10^{60}$ ergs are in kinetic energy, and $\sim 6.6 \times 10^{60}$ ergs are in thermal energy, respectively. In order to explain the lobe radius by this magnetically dominated lobe system, an axial current $\sim 5 \times 10^{17}$ A, which is flowing along the jet central axis, is needed.

5. CONCLUSIONS

By performing 3D MHD simulations, we have investigated the nonlinear dynamics of magnetic tower jets in a galaxy cluster environment. In this fourth paper of the series, we

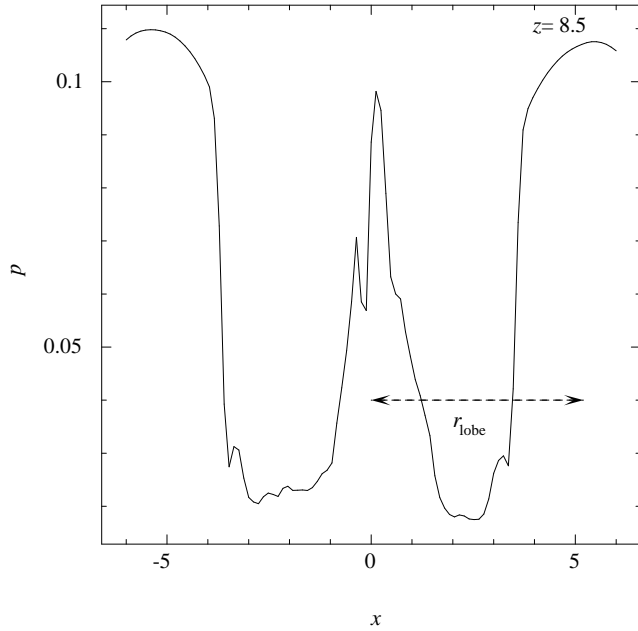


FIG. 6.— Transverse profile in the x -direction of the gas pressure p on $z = 8.5$ (255 kpc). The lobe radius r_{lobe} calculated via eq. (5) is also shown. The pressure cavity radius and r_{lobe} qualitatively agree with each other.

have applied our numerical modeling of the magnetic tower to a specific source, Hercules A.

To our knowledge, this is the first trial of discussing Hercules A jet by using a magnetohydrodynamic model. Projected magnetic field distributions associated with the jets and lobes of Hercules A have been revealed in recent radio observation and therefore, the dynamics including magnetic fields plays a role in understanding this source. In the present paper, we have investigated the jet-driven shock, jet/lobe transition, wiggling, and projected magnetic field distribution of Hercules A and, in general, these features can be explained by our magnetic tower model.

Our conclusions are summarized as follows:

1. A transition from the narrow jet to the fat lobe can occur at the cluster core radius. This interesting feature can also be confirmed in recent observations (Gizani & Leahy 2003, 2004). In our models, the tightly collimated helical field configuration of a magnetic tower jet expands abruptly beyond the core radius due to the decreasing external gas pressure. Thus, the pressure profile of the surrounding ICM plays an important role in determining the morphology of a magnetic tower jet.

2. The expanding magnetic tower jet produces the preceding hydrodynamic shock wave in the ambient ICM. This can be interpreted as AGN-driven shock in X-ray observation and the derived shock Mach number is identical to Nulsen et al. (2005)'s observation result. The magnetic tower lobes expand subsonically and thus no hot spots are produced at the end parts of lobes. This may be a general understanding of FR I or low power FR II radio galaxies (Kraft et al. 2006).
3. The size of the magnetic tower lobe can be accurately estimated from the jet axial current and the external gas pressure at the lobe edge. The estimated lobe size derived by our numerical simulation is qualitatively comparable with the physical scale seen in Gizani & Leahy (2003). In our model, if the background gas has a steep slope (β) in the King profile, the magnetic jet can potentially lead to a huge magnetic tower lobe.
4. Magnetic tower jets, which have a reversed magnetic pinch profile, are subject to current-driven instabilities. Specifically, the apparent distortions by the non-axisymmetric kink mode are visible at the jet body inside the lobe rather than the central core. By expanding the lobe the edge of axial currents could be free against the exciting external kink mode; this situation may be suppressed inside the cluster core radius.
5. The synthetic polarimetry of our magnetic-tower jets is consistent with the gross polarization features observed in the jets of Hercules A. The magnetic tower model produces projected \mathbf{B} -vector distributions that are similar to those observed in the global extragalactic jet-lobe system, especially along the jets and the lobe edges.
6. Magnetic tower jets may produce a self-consistent picture of the field configuration discussed in several non-dynamical model of FR I jets. It consists of toroidally dominated spine inside the lobe and poloidally dominated sheath at the lobe edge (a closed poloidal magnetic flux with a toroidal magnetic component, rather than one side directed helical configuration).

Helpful discussions with Philipp Kronberg and Steven Diehl are gratefully acknowledged. The authors thank the anonymous referee for helpful suggestions. This work was carried out under the auspices of the National Nuclear Security Administration of the U.S. Department of Energy at Los Alamos National Laboratory under Contract No. DE-AC52-06NA25396. It was supported by the Laboratory Directed Research and Development Program at LANL and by IGPP at LANL.

REFERENCES

- Alexander, P. & Leahy, J. P. 1987, MNRAS, 225, 1
 Benford, G. 1978, MNRAS, 183, 29
 Benford, G. 2006, MNRAS, 369, 77
 Bridle, A. H., & Perley, R. A. 1984, ARA&A, 22, 319
 Cavaliere, A., & Fusco-Femiano, R. 1976, A&A, 49, 137
 Churazov, E., Sunyaev, R., Forman, W., & Böhringer, H. 2002, MNRAS, 331, 545
 Croston, J. H., Hardcastle, M. J., Birkinshaw, M., & Worrall, D. M. 2003, MNRAS, 346, 1041
 Clarke, D. A., Norman, M. L., & Burns, J. O. 1989, ApJ, 342, 700
 Clarke, D. A., Bridle, A. H., Burns, J. O., Perley, R. A., & Norman, M. L., 1992, ApJ, 385, 173
 Dreher, J. W., & Feigelson, E. D. 1984, Nature, 308, 43
 Forman, W. et al. 2005, ApJ, 635, 894
 Fabian, A. et al. 2006, MNRAS, 366, 417
 Falle, S. A. E. G. 1991, MNRAS, 250, 581
 Fanaroff, B & Riley, J. M. 1974, MNRAS, 167,31
 Ferrari, A. 1998, ARA&A, 36, 539
 Freidberg J. P. 1982, Rev. Mod. Phys., 54, 801
 Gizani, N. A. B., & Leahy, J. P. 2003, MNRAS, 342, 399 (GL03)

- Gizani, N. A. B., & Leahy, J. P. 2004, MNRAS, 350, 865 (GL04)
- Gooch, R. E. 1995, in ASP Conf. Ser. 101, *Astronomical Data Analysis Software and Systems V*, ed. G. H. Jacoby & J. Barnes (San Francisco: ASP), 80
- Hardee, P. E., & Rosen, A. 1999, ApJ, 524, 650
- Hardee, P. E., & Rosen, A. 2002, ApJ, 576, 204
- Hsu, S. C., & Bellan, P. M. 2002, MNRAS, 334, 257
- Jones, T. W., O'Dell, S. L., & Stein, W. A. 1974, ApJ, 188, 353
- Jones, C., & Forman, W. 1984, ApJ, 276, 38
- Kato, Y., Hayashi, M. R., & Matsumoto, R. 2004, ApJ, 600, 338
- Kato, Y., Mineshige, S., & Shibata, K. 2004, ApJ, 605, 307
- King, I. 1972, ApJ, 174, L123
- Kraft R. P., et al. 2003, ApJ, 592, 129
- Kraft R. P., Azcona, J., Forman, W. R., Hardcastle M. J., Jones, C., & Murray, S. S. 2006, ApJ, 639, 753
- Kudoh, T., Matsumoto, R., & Shibata, K. 2002, PASJ, 54, 26
- Laing, R. A. 1981, ApJ, 248, 87
- Laing, R. A., Canvin, J. R., & Bridle, A. H. 2006, Astron. Nachr. 327, No. 5/6, 523
- Lebedev, S. V. et al. 2005, MNRAS, 361, 97
- Li, H., Lovelace, R. V. E., Finn, J. M., & Colgate, S. A. 2001, ApJ, 561, 915
- Li, S., & Li, H. 2003, Technical Report, LA-UR-03-8935, Los Alamos National Laboratory
- Li, H., Lapenta, G., Finn, J. M., Li, S., & Colgate, S. A. 2006, ApJ, 643, 92 (Paper I)
- Lynden-Bell, D. 1996, MNRAS, 279, 389
- Lynden-Bell, D., & Boily, C. 1994, MNRAS, 267, 146
- Lovelace, R. V. E., Li, H., Koldoba, A. V., Ustyugova, G. V., & Romanova, M. M. 2002, ApJ, 572, 445
- Lovelace, R. V. E., & Romanova, M. M. 2003, ApJ, 596, L159
- Mason, A., Morrison, P., & Sadun, A. C. 1988, Nature, 333, 640
- McNamara, B. R., et al. 2000, ApJ, 534, L135
- McNamara, B. R., et al. 2001, ApJ, 562, L149
- Meier, D. L., Sadun, A. C., & Lind K. R. 1991, ApJ, 379, 141
- Meier, D. L., Koide, S., & Uchida, Y. 2001, Science, 291, 84
- Miley, G. 1980, ARA&A, 18, 165
- Morganti, R., Fanti, R., Gioia, I. M., Harris, D. E., Parma, P., & Ruitter, H. 1988, A&A, 189, 11
- Morrison, P., & Sadun, A. C. 1996, MNRAS, 278, 265
- Muxlow, T. W. B. & Garrington, S. T. 1991 *Beams and Jets in Astrophysics* (New York: Cambridge University Press), 52–99
- Nakamura, M., Li, H., & Li, S. 2006, ApJ, 652, 1059 (Paper II)
- Nakamura, M., Li, H., & Li, S. 2007, ApJ, 656, 721 (Paper III)
- Nulsen, P. E. J., et al. 2005, ApJ, 625, L9
- Romanova, M. M., Ustyugova, G. V., Koldoba, A. V., Chechetkin, V. M., & Lovelace, R. V. E. 1998, ApJ, 500, 703
- Rybicki, G. B., & Lightman, A. P. 1979, *Radiative Process in Astrophysics* (New York: John Wiley and Sons, Inc.)
- Sadun, A. C., & Hayes, J. J. E. 1993, PASP, 105, 379
- Sadun, A. C., & Morrison, P. 2002, ApJ, 123, 2312
- Saxton, C. J., Bicknell, G. V., & Sutherland, R. S. 2002, ApJ, 579, 176
- Scheuer, P. A. G. 1974, MNRAS, 166, 513
- Siebert, J., Kawai, N., & Brinkmann, W. 1999, A&A, 350, 25
- Tregillis, I. L., Jones, T. W., & Ryu, D. 2001, ApJ, 557, 475
- Tregillis, I. L. 2002, Ph.D thesis, U. of Minnesota
- Tregillis, I. L., Jones, T. W., & Ryu, D. 2004, ApJ, 601, 778
- Turner, N. J., Bodenheimer, P., & Różyczka M. 1999, ApJ, 524, 12
- Ustyugova, G. V., Lovelace, R. V. E., Romanova, M. M., Li, H., Colgate, S. A. (2000), ApJ, 541, L21
- Uzdensky, D. A., & MacFadyen, A. I. 2006, ApJ, 647, 1192
- Vikhlinin, A., Markevitch, M., & Murray, S. S. 2001, ApJ, 549, L47